J. Fluid Mech. (1992), *vol.* 236, *pp.* 1–26
Printed in Great Britain

Mixing by chaotic advection in a class of spatially periodic flows

By SUSAN C. RYRIE
School of Mathematics, University Walk, Bristol BS8 1TW, UK

(Received 28 March 1989 and in revised form 29 July 1991)

The paths followed by individual fluid particles can be extremely complicated even in smooth laminar flows. Such chaotic advection causes mixing of the fluid. This phenomenon is studied analytically for a class of spatially periodic flows comprising a basic flow of two-dimensional (or axisymmetric) counter-rotating vortices in a layer of fluid, and modulated by a perturbation which is periodic in time and/or space. Examples of this type of flow include Bénard-convection just above the point of instability of two-dimensional roll cells, and Taylor vortex flow between concentric rotating cylinders. The transport of chaotically advected particles is modelled as a Markov process. This predicts diffusion-like mixing, and provides an expression for the diffusion coefficient. This expression explains some features of experimental results reported by Solomon & Gollub (1988): its accuracy is investigated through a detailed comparison with numerical results from a model of wavy Taylor vortex flow. The approximations used in the analysis are equivalent to those used to obtain the quasi-linear result for diffusion in the standard map.

1. Introduction

Chaotic advection in fluid flow has been the subject of much research in recent years. This phenomenon manifests itself when one studies the paths, $\boldsymbol{x}(t)$, followed by individual fluid particles. These are given by

$$\frac{\mathrm{d}\boldsymbol{x}}{\mathrm{d}t} = \boldsymbol{u}(\boldsymbol{x}, t), \tag{1.1}$$

where $\boldsymbol{u}(\boldsymbol{x}, t)$ is the Eulerian velocity field of the fluid. Then the theory of dynamical systems shows that the solutions may be chaotic, even for simple (albeit nonlinear) functions $\boldsymbol{u}$. Thus chaotic particle paths may occur even in smooth laminar flows. This was first described by Arnol'd (1965) and Hénon (1966), and called chaotic advection by Aref (1984). Recent reviews of the phenomenon have been provided by Ottino (1989, 1990).

The effect of chaotic advection is to cause mixing of the fluid. This is illustrated in, for example, the theoretical work of Dombre *et al.* (1986), and the experimental work of Chaiken *et al.* (1986) and Ottino *et al.* (1988); for further discussion and references see, again, Ottino (1989, 1990). The nature of this mixing in a simple model of wavy Taylor vortex flow between concentric rotating cylinders was studied numerically by Broomhead & Ryrie (1988). In the basic flow of steady, axisymmetric vortices there are only well-ordered particle paths, confined to invariant toroidal surfaces. However, when a time-periodic perturbation, such as one which might

model an instability of this flow, is added, the dividing streamlines between adjacent vortices are broken. This leads to chaotic advection, and transport of particles between neighbouring vortices. Broomhead & Ryrie showed numerically that the transport of particles along the length of the cylinders can be characterized as a diffusion process, with diffusion coefficient varying with the strength of the perturbation. Note that this diffusion-like behaviour is of macroscopic origin, and occurs even in the absence of molecular diffusion.

Similar results were found by Solomon & Gollub (1988), who studied particle transport experimentally and numerically in two-dimensional, time-dependent Rayleigh–Bénard convection. This flow is qualitatively similar to the Taylor vortex flow studied by Broomhead & Ryrie (1988). In the basic steady flow particles are confined to the closed streamlines of two-dimensional roll cells: the time-dependent perturbation breaks dividing streamlines between adjacent cells, allowing transport of particles along the layer. Solomon & Gollub (1988) found that the transport could be described as a one-dimensional diffusive process; moreover that the effective diffusion coefficient varied linearly with the strength of the time-dependent component of the flow. Their results were independent of the molecular diffusivity of the tracer particles used, indicating that mixing by chaotic advection is the dominant effect over the range of molecular diffusivities which they used.

Further numerical studies of transport due to chaotic advection in similar types of flows have been carried out by Weiss & Knobloch (1989) and Cox *et al.* (1990). These were motivated, respectively, by modulated travelling waves in binary-fluid mixtures, and by Rossby wave flow in the atmosphere. However, unlike the examples considered by Broomhead & Ryrie (1988) and Solomon & Gollub (1988), these flows exhibit a net flux of fluid along the layer. This flux manifests itself in the basic flow by the presence of a unidirectional stream winding between the vortices. The effect of this net flux upon the transport properties of the flow is to produce anomalous diffusion, whereby the mean-square displacement of particles, $\Delta x^2(t)$, satisfies

$$\Delta x^2(t) \sim t^\nu \quad \text{as} \quad t \to \infty,$$

where $\nu > 1$; for diffusion-limited transport $\nu \equiv 1$.

The aim of this paper is to demonstrate the origin of the diffusion-like transport observed in the above studies of flows with no net flux, and to obtain an approximate expression for the diffusion coefficient. Whereas most previous investigations have been essentially numerical, by making appropriate approximations we are able to treat the problem analytically. The flow is assumed to consist of a single (infinite) row of cells (or counter-rotating vortices), subject to a temporally periodic perturbation. This general formulation embraces a wide range of flows, including the two examples of Taylor-vortex flow and Bénard convection mentioned above. Following ideas used by Meiss and co-workers (MacKay, Meiss & Percival 1984; Meiss 1986; Meiss & Ott 1986) in their studies of transport in two-dimensional mappings, we calculate the flux of particles across cell boundaries, and model the transport as a Markov process. This indeed predicts diffusion-like transport, and provides an expression for the effective diffusion coefficient. This analytic expression is compared with numerical results from the model studied by Broomhead & Ryrie (1988). Additionally, the Markov model suggests that the anomalous diffusion observed in the cases of flows with non-zero net flux may be caused by shear within the flows, rather than by the net flux itself.

During the course of this work we learnt that similar ideas had independently been applied to the study of chaotic advection in fluid flows by Rom-Kedar (1989) (see

also Rom-Kedar, Leonard & Wiggins 1990). However, there the detailed structure of the transfer mechanism across broken cell boundaries, and of the trapping and escape of particles is investigated. In contrast, in this paper, by adopting the Markov model, we ignore many details of the transport process in favour of obtaining a simple first approximation to the diffusion coefficient.

The weakness of the Markov model approximation lies in assuming that the particles 'forget' their previous history after just one period of the flow. However, since it is well known that the autocorrelation functions of chaotic signals decay to zero (cf. Ottino 1989, p. 129), we expect this approximation to be good in cases where the timescale of this decay is sufficiently small compared with the period of the flow. It is important to remember though, that in other cases correlation effects may be important and cause discrepancies between our approximate analytic result and the true value of the diffusion coefficient. Some discrepancies which are probably attributable to this cause will be seen, as well as some remarkably good agreement, in our comparison between the analytic approximation and numerical results. The complexity of these higher-order correlation effects can be seen in the work of Rom-Kedar (1989) and Rom-Kedar *et al.* (1990). To include them in a calculation of the diffusion coefficient is beyond the scope of the present work. As indicated above, we choose instead to ignore them in order that we may obtain a simple first-order approximation.

Although the investigation of transport due to chaotic particle paths is fairly new in the context of fluid dynamics, transport properties of chaotic two-dimensional, area-preserving maps have been studied for some time (cf. Lichtenberg & Lieberman 1983, 1988; MacKay *et al.* 1984; Meiss 1986, Meiss & Ott 1986). When we recall that for convenience a flow is often reduced to such a map – the Poincaré map which in periodic two-dimensional flow of an incompressible fluid, for example, relates the positions of fluid particles at successive time intervals equal to one period of the flow – we might expect that the methods used in the studies of mappings could be applied directly to the case of fluid flow. However, there are some important differences. First, the explicit form of the Poincaré map cannot, in general, be obtained from the flow field. Secondly, as Weiss & Knobloch (1989) discuss, the mappings are usually expressed in action-angle coordinates, with the diffusion occurring in the action variable. In contrast, the fluid flow is not normally in action-angle form, and the diffusion occurs in real space. Although these differences prevent direct application of the methods used in the study of mappings, they do not appear to significantly affect the diffusion process, and many features of diffusion in mappings are seen in the numerical results of diffusion in chaotic fluid flows. Moreover, as our appeal to the ideas of Meiss and co-workers exemplifies, the philosophy of the methods can often be of use.

Of particular interest is the work on diffusion in the 'standard map': this is reviewed by Lichtenberg & Lieberman (1983). An analytic expression for the diffusion coefficient can be derived in the form of an infinite series. A first approximation, the 'quasi-linear result', is found by assuming that particles have no memory of their past history. This is equivalent to the Markov process approximation which we adopt in this paper. Higher-order corrections lead to oscillations about the quasi-linear result, which decay as the parameter governing the nonlinearity of the map increases to infinity. Our results for the model of wavy Taylor-vortex flow show a similar behaviour: the numerical results oscillate about the analytic approximation for small perturbations, but tend to the same value as the amplitude of the perturbation becomes 'large'.

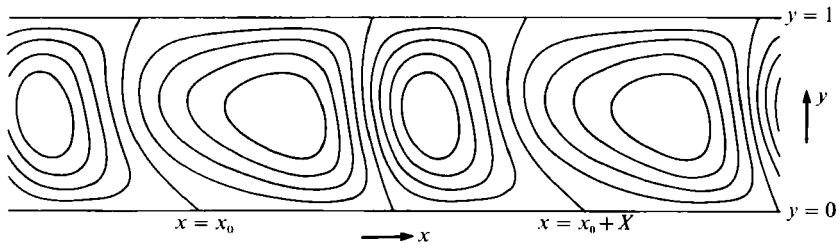

FIGURE 1. General topological form of the streamlines in the unperturbed flow ($\epsilon = 0$). Note that the two (counter-rotating) cells in each spatial period of the flow need not be of the same shape or size.

It is important to recognize that throughout this paper we ignore the effects of molecular diffusion. Of course, molecular diffusion will always be present in real fluid flows. Nevertheless, the work of Solomon & Gollub (1988) suggests that its effects are small compared with those of chaotic advection in at least some cases of practical interest. Additionally, the rapid mixing caused by the chaotic advection should not be confused with the enhancement of molecular diffusion by the spatial structure of *axisymmetric* Taylor vortices, and *steady* Rayleigh–Bénard convection. This phenomenon has been investigated by Sagues & Horsthemke (1986) and Young, Pumir & Pomeau (1989). Once molecular diffusion has carried particles across one dividing streamline, they are rapidly transported by the flow to the next vortex boundary, which again can only be crossed by molecular diffusion. This contrasts with the cases we study here, in which the breaking of the symmetry of the flow causes the dividing streamlines themselves to be broken; it is the action of the flow itself which carries particles between adjacent vortices, even when there is no molecular diffusion.

2. Description of the flow

Consider a steady two-dimensional flow of an incompressible fluid, such that the streamlines are topologically equivalent to those shown in figure 1 (three-dimensional flows in which the velocity field is independent of the third spatial coordinate, z, can be analysed in a similar way, as will be discussed in §4). The flow is bounded in y, and consists of a series of cells periodically spaced in x. Ideal fluid particles follow paths $\boldsymbol{x}(t) = (x(t), y(t))$ given by

$$\frac{\mathrm{d}x}{\mathrm{d}t} = \psi_y(x, y), \quad \frac{\mathrm{d}y}{\mathrm{d}t} = -\psi_x(x, y), \tag{2.1}$$

where $\psi(x, y)$, the stream function, has period X in x, and satisfies

$$\psi(x, 0) = \psi(x, 1) = 0$$

for all x, in order that there be no flow across the boundaries $y = 0$ and $y = 1$, and no net flux along the layer. Stagnation points lie at periodic intervals along the boundaries, where $\nabla\psi = 0$. These stagnation points are of saddle type: each has a stable manifold comprising all initial positions which are asymptotic to the saddle point as $t \to +\infty$, and an unstable manifold comprising all initial positions asymptotic to the saddle point as $t \to -\infty$. Thus the stable and unstable manifolds correspond, respectively, to curves of inflow and outflow of fluid. Note that particles are unable

to cross such manifolds. This property is fundamental to the mechanism whereby a small perturbation to equations (2.1) may give rise to flow with chaotic particle paths, and to our analysis of the resultant transport. In this particular case, the manifolds of adjacent stagnation points coincide, joining these points along the boundaries of the flow, and along the dividing streamlines which separate neighbouring vortices. Thus each cell boundary comprises a 'heteroclinic cycle'. Such a configuration is structurally unstable and likely to be broken by small perturbations of the system.

When the forcing of the fluid system is increased beyond a critical value, the basic flow described above often becomes unstable to a time-periodic perturbation (cf. Davey, DiPrima & Stuart 1968; Clever & Busse 1974). Then particles paths are described by equations of the form:

$$\left.\begin{aligned} \frac{\mathrm{d}x}{\mathrm{d}t} &= \psi_y(x,y) + \epsilon g_y(x,y,t), \\ \frac{\mathrm{d}y}{\mathrm{d}t} &= -\psi_x(x,y) - \epsilon g_x(x,y,t), \end{aligned}\right\} \tag{2.2}$$

where g has period X in x, and T in t. This form of the perturbation automatically satisfies the continuity equation for the incompressible fluid. In addition we impose $g(x,0,t) = g(x,1,t) = 0$ for all x and t, in order to preserve the boundaries at $y = 0$ and $y = 1$, and the condition of no net flux along the x-axis. Standard methods are available to study the solutions to equations of this form. We briefly outline those results necessary for our discussion of diffusion in the perturbed flow. For further details see, for example, Guckenheimer & Holmes (1983), or, for a discussion in the context of wavy Taylor vortex flow, Broomhead & Ryrie (1988).

Solutions to equations (2.2) are conveniently visualized by use of a Poincaré map. This map relates the positions of particles after intervals of time equal to one period of the perturbation: it is equivalent to stroboscopically illuminating the flow. Since the fluid is incompressible, the Poincaré map is area-preserving.

The stagnation points on the boundaries of the unperturbed flow correspond to fixed points of the Poincaré map. It can be shown that, for small enough ϵ, these survive in the Poincaré map of the perturbed flow (though they will in general be displaced by a distance of order ϵ), and retain the same, saddle-type, stability. Correspondingly, the stagnation points of the basic flow are replaced by periodic orbits in the perturbed flow. The boundary conditions ensure that these fixed points of the perturbed map remain in the boundaries $y = 0$ and $y = 1$ of the flow. They have stable and unstable manifolds defined similarly to those of the basic steady flow, but with n, the number of iterations of the map, taking the role of time, t. The boundary conditions ensure that half of these manifolds lie along the fluid boundaries and coincide as in the case of $\epsilon = 0$. No such constraints act on the manifolds which enter into the body of the fluid: in general these no longer coincide, thus causing the dividing streamlines between adjacent cells to be broken, and allowing the migration of particles along the length of the layer. However, the condition of no net flux along the x-axis does require these perturbed manifolds to intersect at least once (cf. Cox *et al.* 1990). It is easy to show that in this case they must intersect an infinite number of times, and so wind 'wildly' in space: this is the origin of the chaotic advection in this class of flow.

Figure 2 shows schematically these perturbed manifolds in a typical case. On

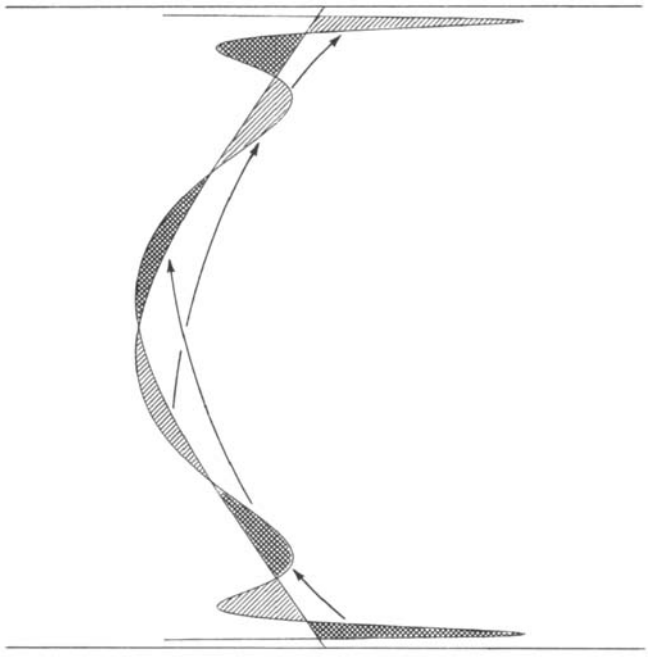

FIGURE 2. Typical form of the perturbed manifolds near a cell boundary. Shaded regions contained between the manifolds are mapped as indicated by the arrows: particles in these regions are able to change cell on moving upwards from $y = 0$ to $y = 1$. A similar structure will occur near the downwards-moving cell boundaries.

approaching the fixed point from which it has broken away, the perturbed manifold oscillates increasingly rapidly and intersects the other manifold an infinite number of times. Since particles are unable to cross these invariant manifolds, areas defined by successive intersections of the manifolds (shaded in figure 2) are mapped into each other as shown in the figure. Thus particles are able to change cell on moving across from one horizontal boundary of the flow to the other.

The separation of the perturbed manifolds, measured at a point (x_0, y_0) on, and in the direction of the normal to, the manifolds of the unperturbed system can be shown to be (Guckenheimer & Holmes 1983, pp. 189–190):

$$d(y_0, t_0; x_0) = \frac{\epsilon M(y_0, t_0; x_0)}{|\nabla\psi(x_0, y_0)|} + O(\epsilon^2) \quad \text{as} \quad \epsilon \to 0, \tag{2.3}$$

where

$$M(y_0, t_0; x_0) = \int_{-\infty}^{\infty} \nabla\psi(x^0(t-t_0), y^0(t-t_0)) \wedge \nabla g(x^0(t-t_0), y^0(t-t_0), t)\, \mathrm{d}t, \tag{2.4}$$

is the Melnikov function, and $(x^0(t), y^0(t))$ is a 'heteroclinic' orbit of the unperturbed system (i.e. an orbit lying in the coincident manifolds of the two fixed points) which passes through (x_0, y_0) at $t = 0$. Here $t_0 \in [0, T)$ is the time on which the Poincaré map is based, and x_0 is a passive parameter in d and M, used to define which cell boundary is referred to. Although it is common to regard (x_0, y_0) as fixed and to study the variation of the Melnikov function with t_0 alone, we prefer here to retain explicitly the variation with y_0. Indeed, for clarity, we shall rather regard t_0 as fixed, and study the variation of the separation of the manifolds with y_0: the two approaches are equivalent (Guckenheimer & Holmes, 1983, p. 189). If $d(y_0, t_0; x_0)$, through the

Melnikov function, has successive (simple) zeros in y_0 at $y_0 = y_i$ and $y_0 = y_{i+1}$, then the perturbed manifolds intersect transversely near $(x, y) = (x_0, y_i)$ and (x_0, y_{i+1}). The area of the region defined by these intersections is then

$$a(i; x_0) = \int_{\lambda(y_i)}^{\lambda(y_{i+1})} |d(y_0(\lambda), t_0; x_0)| \, \mathrm{d}\lambda = \epsilon \int_{t_i}^{t_{i+1}} |M(y_0, t_0; x_0)| \, \mathrm{d}t + O(\epsilon^2) \quad \text{as} \quad \epsilon \to 0, \quad (2.5)$$

where λ is the distance measured along the heteroclinic orbit of the unperturbed system and $y^0(t_i) = y_i, y^0(t_{i+1}) = y_{i+1}$, and where we have used

$$\mathrm{d}\lambda/\mathrm{d}t = |\nabla\psi(x_0, y_0(\lambda))|.$$

Since the Poincaré map is area-preserving, and there is no net flux along the layer, we have respectively

$$a(i+2; x_0) = a(i; x_0), \quad a(i+1; x_0) = a(i; x_0). \quad (2.6)$$

Thus all areas $a(i; x_0)$ are equal for a given x_0. They are independent of the section time t_0, and in this case of no net flux can be calculated from (2.5) with t_i and t_{i+1} taken to be any two adjacent zeros in t_0 of M. These expressions for $a(i; x_0)$ will be used to estimate the number of particles changing cell in a given time, and, ultimately, a diffusion coefficient for the transport of particles. Rom-Kedar (1989) has independently used the same formulation to study the detailed structure of the transfer mechanism across the broken vortex boundary.

In order to move between adjacent cells, particles must visit the neighbourhood of the cell boundaries. However, for small enough ϵ, many of the closed streamlines of the steady flow are preserved (though distorted) in the Poincaré section, and continue to confine particle paths. These closed, invariant curves are known as KAM tori; particles within a KAM torus are confined indefinitely to the core of the cell, away from the boundaries. Thus it is only particles in an outer region, which Rom-Kedar (1989) calls the 'mixing region', that are free to travel along the layer. As ϵ is increased, the mixing region generally grows whilst the inner trapped region shrinks until the last KAM torus is destroyed. However, the picture is complicated by the possibility of 'islands' of trapped particles, and of 'cantori' which present partial barriers to particle transport appearing and disappearing in the mixing region as ϵ is varied. Consequently the size of the mixing region does not necessarily increase monotonically, or smoothly. Examples of Poincaré maps which illustrate these effects in this class of flow can be found in Broomhead & Ryrie (1988), Solomon & Gollub (1988), Weiss & Knobloch (1989) and Cox *et al.* (1990). The presence of cantori causes slow leakage of particles between different parts of the mixing region, and can profoundly affect the overall transport of particles. It is intimately related to the existence of the high-order correlation effects which were discussed in §1: to include these effects is beyond the scope of this work and we will thus assume that the mixing region is well-defined and does not contain cantori.

Throughout this section we have assumed free-slip at the fluid boundaries $y = 0$ and $y = 1$. This ensures that the stagnation points there are hyperbolic, i.e. their stability can be determined by linearizing the flow. This is a necessary condition for the straightforward application of the results which we have used from the theory of dynamical systems. In particular, it guarantees the preservation of the stagnation points under a small perturbation of the system. However, in many cases of interest the boundaries may support no-slip; then the stagnation points are non-hyperbolic and more care is needed. Broomhead & Ryrie (1988) discuss the implications of this on the existence of fixed points and manifolds in the perturbed Poincaré map.

Although the continued existence of non-hyperbolic fixed points under a perturbation of the system cannot be guaranteed in general, in this particular class of flows the symmetry and the condition of no net flux along the layer limit the class of admissible perturbations, and guarantee the continued existence of the saddle points and their manifolds, at least under 'small' perturbations of the basic flow. Moreover, numerical studies show no apparent qualitative difference between flows with the two types of boundary conditions so that we expect the above discussion to apply equally well in either case. However, it would be a valuable and interesting extension of this work to investigate this point further.

3. Diffusion properties

The boundary between adjacent cells in the unperturbed flow is formed from the stable and unstable manifolds of the stagnation points. It is convenient to define the boundary between cells in the perturbed flow as also lying along manifolds of the periodic orbits. Thus we consider the Poincaré map based at time $t = t_0$, and select a point of intersection of the perturbed manifolds which lies near the centre of the layer of fluid. Above this point of intersection, the boundary is taken to lie along the manifold of the fixed point at the upper fluid surface; below this point it is taken to lie along the manifold of the fixed point on the lower surface of the fluid (see figure 3, cf. MacKay *et al.* 1984, figure 11).

Near the upper and lower surfaces of the fluid, the cell boundary forms an impenetrable barrier in the Poincaré section, since particles are unable to cross the manifolds of which it is formed. However, near the centre of the layer, particles are able to 'leak' through by entering the regions marked $I_{i,j}$ in figure 3; under the action of the Poincaré map they are then mapped across the boundary into the neighbouring cell. The suffices i and j are used to denote that particles in the region $\mathrm{I}_{i,j}$ are mapped from cell i to cell j under one iteration of the Poincaré map. This behaviour is directly analogous to the leaking of particles across cantori (the remnants of periodic orbits), as described by MacKay *et al.* (1984): the boundaries of regions $\mathrm{I}_{i,j}$ are the 'turnstiles' controlling the escape of particles.

Consider now the fate of tracer particles being advected by the flow. Then the change in the number of particles in cell i during one period of the flow is given by

$$N_i(t+T) = N_i(t) + n_{i-1,i}(t) + n_{i+1,i}(t) - n_{i,i-1}(t) - n_{i,i+1}(t), \tag{3.1}$$

where $N_i(t)$ is the number of particles in cell i at time t, and $n_{i,j}(t)$ is the number of particles in region $\mathrm{I}_{i,j}$ at time t. On writing $N_i(t) = N_i^{\mathrm{t}} + N_i^{\mathrm{m}}(t)$, where N_i^{t} is the (constant) number of particles in the trapped region of cell i, and $N_i^{\mathrm{m}}(t)$ the number of particles in the mixing region of cell i, we see that $N_i(t)$ in (3.1) can be replaced by $N_i^{\mathrm{m}}(t)$. Henceforth we will consider only particles in the mixing regions of the flow. Following Meiss (1986), we note that those particles free to cross the cell boundary lie within a stochastic region of the flow, and so quickly forget their past history. We will assume here, in order to obtain a first approximation to the transport problem, that particles immediately forget their past on crossing a cell boundary, and are quickly distributed throughout the mixing region. Then we approximate $n_{i,j}(t)$ as

$$n_{i,j}(t) = N_i^{\mathrm{m}}(t)\, a_{i,j}/A_i, \tag{3.2}$$

where A_i is the area of the mixing region in cell i, and $a_{i,j}$ is the area of region $I_{i,j}$. Note that the condition of no net flux along the layer gives

$$a_{i,j} = a_{j,i}.$$

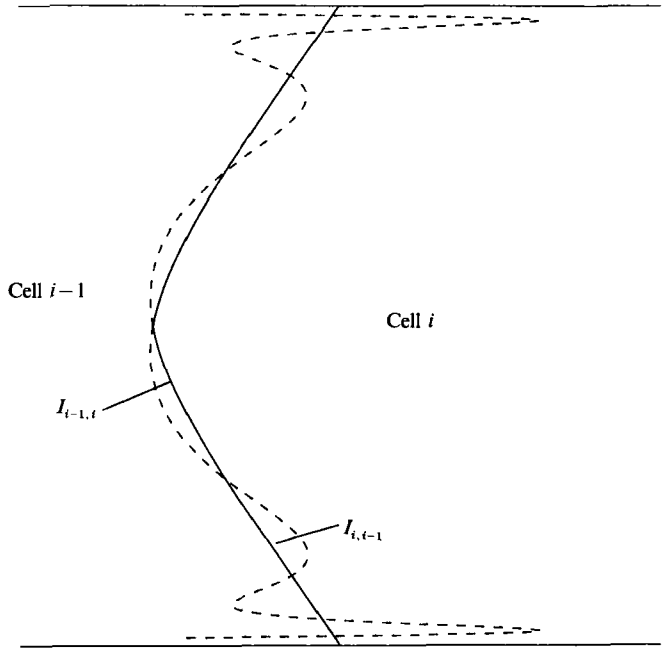

FIGURE 3. The definition of the cell boundary (solid line) in the perturbed flow. The dashed line show the positions of the perturbed manifolds, and the regions $I_{i,j}$ the areas of the turnstiles through which particles move from one cell to another.

On substituting for $n_{i,j}(t)$ from (3.2) into (3.1), we have

$$\frac{N_i^{\mathrm{m}}(t+T)}{A_i}-\frac{N_i^{\mathrm{m}}(t)}{A_i}=\frac{a_{i+1,i}}{A_i}\frac{N_{i+1}^{\mathrm{m}}(t)}{A_{i+1}}-\frac{(a_{i,i+1}+a_{i,i-1})}{A_i}\frac{N_{i(t)}^{\mathrm{m}}}{A_i}+\frac{a_{i-1,i}}{A_i}\frac{N_{i-1}^{\mathrm{m}}(t)}{A_{i-1}}. \tag{3.3}$$

This is a discrete form of the advection–diffusion equation

$$\frac{\partial(N_i^{\mathrm{m}}/A_i)}{\partial t}+u_i\frac{\partial(N_i^{\mathrm{m}}/A_i)}{\partial x}=D_i\frac{\partial^2(N_i^{\mathrm{m}}/A_i)}{\partial x^2}, \tag{3.4}$$

where

$$u_i=\frac{X}{2T}\frac{(a_{i+1,i}-a_{i,i-1})}{A_i}, \tag{3.5}$$

and, depending on whether the first derivatives are defined by upwind, downwind or central differences respectively,

$$\frac{4T}{X^2}D_i=\frac{a_{i-1,i}}{A_i},\quad \frac{a_{i+1,i}}{A_i}\quad \text{or}\quad \frac{(a_{i+1,i}+a_{i-1,i})}{2A_i}. \tag{3.6}$$

In general, $a_{i+1,i}\neq a_{i,i-1}$, so that the advection velocity u_i is non-zero. This is not inconsistent with the condition of no net flux along the layer, since here we are considering only the change of particles in cell i. On replacing i by $i+1$ in (3.4)–(3.6), and using $a_{i+2,i+1}=a_{i,i-1}$, we find the equation governing the change of particles in cell $i+1$. This has an advection velocity $u_{i+1}=-A_iu_i/A_{i+1}$ in the opposite sense to that in cell i, so that on average the two may be expected to cancel. The phenomenon is easily understood when we recall that the $a_{i,j}$ denote the areas of the turnstiles which control the exchange of particles between cells: small turnstiles admit only a slow migration of particles and so form 'high' barriers which are difficult to cross,

while large turnstiles form 'low' barriers which particles may cross easily. When $a_{i+1,i} \neq a_{i,i-1}$, successive cell boundaries have alternately large and small turnstiles. Particles 'pile up' behind the high barriers (small turnstiles) thereby causing the alternating positive and negative advection velocities in adjacent cells.

Equation (3.4) indicates that on lengthscales much greater than X and timescales much greater than T, the transport of particles along the layer is approximately governed by an advection–diffusion equation. However, the inverse problem of deriving the value of the diffusion coefficient from the discrete form (3.3) does not have a unique solution; we find three possible values of D_i, and three of D_{i+1}, all of which are generally different when $a_{i+1,i} \neq a_{i,i-1}$ and $A_i \neq A_{i+1}$. Therefore we must use an alternative method. Following Meiss (1986). we model the transport of particles by a Markov chain, and calculate the variance of the distribution. In a diffusive process this varies linearly with the number of steps (here the number of iterations of the Poincaré map, and hence time), the constant of proportionality determining the diffusion coefficient.

Therefore, suppose that during one iteration of the Poincaré map all particles in the mixing region of cell i are equally likely to cross the boundary to cell $i \pm 1$, with probability

$$P_{i,i\pm1} = a_{i,i\pm1}/A_i. \tag{3.7}$$

This approximation assumes that particles 'forget' their previous history after each iteration of the Poincaré map: it is equivalent to the approximation made in (3.2), and to the 'quasi-linear' approximation made in early studies of diffusion in the standard map. Of course it is not exact, as the work of Rom-Kedar (1989) and Rom-Kedar *et al.* (1990) exemplifies. Nevertheless it allows us to derive a first approximation to the diffusion coefficient which, in some cases, is in very good agreement with numerically calculated values.

So writing

$$\left.\begin{aligned} \rho &= P_{2r,r+1} = a_{2r,2r+1}/A_{2r}, \\ \lambda &= a_{2r,2r-1}/a_{2r,2r+1}, \\ \mu &= A_{2r}/A_{2r+1}, \end{aligned}\right\} \tag{3.8}$$

the probability of a particle migrating from cell i to cell j in one 'step' is

$$P_{i,j} = \left.\begin{aligned} &(1-\rho-\lambda\rho)\,\delta_{j,i} + \rho\delta_{j,i+1} + \lambda\rho\delta_{j,i-1}, && i \text{ even} \\ &(1-\mu\rho-\mu\lambda\rho)\,\delta_{j,i} + \mu\lambda\rho\delta_{j,i+1} + \mu\rho\delta_{j,i-1}, && i \text{ odd}, \end{aligned}\right\} \tag{3.9}$$

where $\delta_{j,i}$ is the Kronecker delta ($\delta_{j,i} = 1$ if $j = i$, $\delta_{j,i} = 0$ *if* $j \neq i$).The distribution after 10 steps is compared with a Gaussian distribution in figure 4: part (*b*) clearly shows particles 'piling up' behind the small turnstiles when $(\lambda, \mu) \neq (1, 1)$.

The variance of the distribution of this process after a fixed number, n, of iterations of the map is calculated in the Appendix. For large n, we find

$$\langle (i-i_0)^2 \rangle_n - \langle i-i_0 \rangle_n^2 \sim 2D'_{\mathrm{M}} n \quad \text{as} \quad n \to \infty, \tag{3.10}$$

where

$$D'_{\mathrm{M}} = \frac{2\mu}{(1+\mu)} \frac{2\lambda}{(1+\lambda)} \rho. \tag{3.11}$$

Thus particles migrate as if diffusing, with diffusion coefficient D'_{M}. This expression for the diffusion coefficient (3.11) is dimensionless with respect to the size of the cells, and the temporal period of the perturbation: the full dimensional form is

$$D_{\mathrm{M}} = \frac{X^2}{4T} D'_{\mathrm{M}} = \frac{X^2}{T} \frac{1}{(A_{2r}+A_{2r+1})} \frac{a_{2r,2r-1}\, a_{2r,2r+1}}{(a_{2r,2r-1}+a_{2r,2r+1})}. \tag{3.12}$$

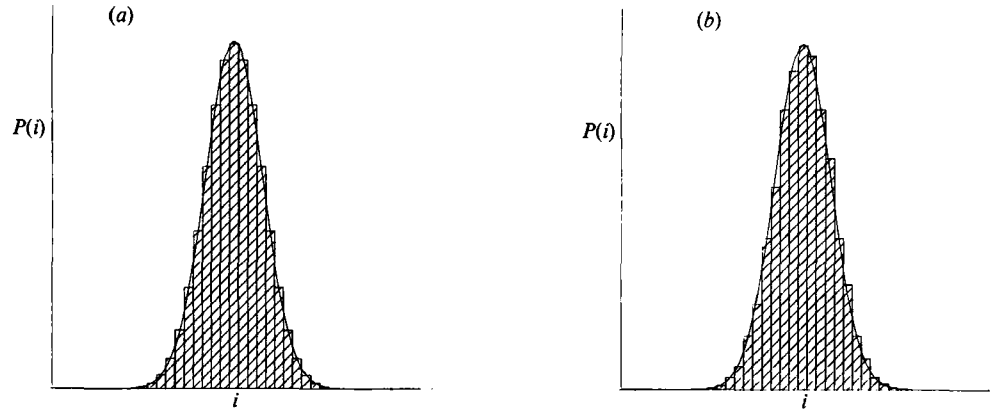

FIGURE 4. Distribution of the process described by equation (3.9) after 10 steps (histogram) compared with Gaussian distribution (smooth curve). (*a*) $(\lambda, \mu, \rho) = (1, 1, \frac{1}{4})$; (*b*) $(\lambda, \mu, \rho) = (1\frac{1}{2}, 1, \frac{1}{5})$.

Note that (3.11) can be rewritten as

$$(D'_{\mathrm{M}})^{-1} = \tfrac{1}{4}(d^{-1}_{i,i+1} + d^{-1}_{i,i-1} + d^{-1}_{i+1,i} + d^{-1}_{i-1,i}), \tag{3.13}$$

where

$$d_{i,j} = a_{i,j}/A_i. \tag{3.14}$$

Thus the inverse of the diffusion coefficient is the mean of the inverses of the coefficients found from the difference formulae (3.6).

Equation (3.12) provides a first approximation to the diffusion coefficient for particles located in the mixing region of the flow. We now consider how this expression is related to numerical and experimental measurements of diffusion coefficients. First note that particles in the trapped regions cannot diffuse, so that the diffusion coefficient there is zero. Thus we see that in a chaotic flow the value of the diffusion coefficient may vary in space. Indeed, it is likely that the value of the diffusion coefficient varies with position even within the mixing region; then expression (3.12) should be interpreted as an approximation to the diffusion coefficient averaged over the whole mixing region. Now recall that experimental and numerical measurements of diffusion coefficients are often based on spatial averages as well, since they normally use ensembles of particles distributed throughout a given, regular, region of the flow. Thus the measured diffusion coefficient is in practice a spatial average of the coefficients at each point in the region. When the measurement region is taken to be one complete wavelength of the flow, the measured diffusion coefficient is γD, where γ is the proportion of the flow which is mixing, i.e. $\gamma = (A_{2r} + A_{2r+1})/A_{\mathrm{tot}}$, and where A_{tot} is the total area of the measurement region. So, in order to compare our theory with numerical or experimental results we should more correctly consider the quantity γD.

In order to estimate γD from (3.12) we need to know values of the quantities X, T, A_{tot} and the $a_{i,j}$, but not of $(A_{2r} + A_{2r+1})$. The first three are generally known explicitly for a given flow, so that the problem reduces to that of determining the $a_{i,j}$. As we have seen in §2, these areas may be calculated in terms of the Melnikov function, through (2.5), provided the perturbation is sufficiently small; for larger perturbations we must resort to numerical measurement. We are now able to explain the linear variation of diffusion coefficient with the size of the perturbation which was observed both experimentally and numerically by Solomon & Gollub (1988). For

small-amplitude perturbations, the $a_{i,j}$ vary linearly with the size of the perturbation as indicated in (2.5). This implies that γD_{M}, our estimate from (3.12) of the measured diffusion coefficient, also varies linearly with the size of the perturbation, in agreement with the observations.

The quantity γ is also important in describing the mixing properties of the flow. However, at present we have no method of estimating its size. This point is discussed further in §7.

It is useful to note that for an ensemble of particles initially distributed evenly throughout a whole number of cells, the change in the number of particles in each cell after just one period of the flow is exactly represented by the Markov model. It is only after further periods of the flow that the correlations effects which we have ignored can enter into the problem. Then from (A 20) of the Appendix, the mean-square displacement of particles after this one step is

$$\langle (i(T)-i(0))^2\rangle = 2D'_{\mathrm{M}} + \frac{\rho(1+\lambda)(1-\mu)}{1+\mu}(\sigma_{\mathrm{e}}^0 - \mu\sigma_{\mathrm{o}}^0) + \frac{2\mu\rho(1-\lambda)^2}{(1+\lambda)(1+\mu)}, \tag{3.15}$$

where λ, ρ and μ are defined in (3.8), and σ_{e}^0 and σ_{o}^0 are defined in (A 8). But σ_{e}^0 is just the probability that a randomly selected particle initially lies in an 'even' cell, and σ_{o}^0 the probability that it initially lies in an 'odd' cell, so that for this particular ensemble $(\sigma_{\mathrm{e}}^0 - \mu\sigma_{\mathrm{o}}^0) = 0$. Thus we find

$$\langle (i(T)-i(0))^2\rangle = \left[2 + \frac{(1-\lambda)^2}{\lambda}\right] D'_{\mathrm{M}}. \tag{3.16}$$

When both cells comprising one spatial period of the flow are identical, such as for flows invariant under the transformations $(x,y,t) \to (x+\frac{1}{2}X, y, -t)$ or $(x,y,t) \to (-x, y, t)$ for example, then $\lambda = 1$. It follows that the diffusion coefficient $\lambda D'_{\mathrm{M}}$ can be calculated numerically by integrating the flow for just one temporal period. This provides an alternative to computing the areas $a_{i,j}$. Since the mean-square deviation in (3.16) varies only slowly with λ, for λ close to 1, this method may also be used to provide a rough estimate of $\gamma D'_{\mathrm{M}}$ for $\lambda \neq 1$: the percentage error when $\lambda = 2$ (or equivalently $\lambda = \frac{1}{2}$, depending on how the origin of the cells is defined) is 25%.

In deriving (3.12), we have used the cell index, $i(t)$, of each particle, whereas in numerical calculations it is often more convenient to use the true coordinate along the layer, $x(t)$. Thus $D_{\mathrm{num}} = \lim_{t\to\infty} d_{\mathrm{num}}(t)$, where

$$\gamma d_{\mathrm{num}}(t) = \frac{\langle (x(t)-x(0))^2\rangle - \langle x(t)-x(0)\rangle^2}{2t}, \tag{3.17}$$

and where $\langle\ \rangle$ denotes an average over the ensemble of sample particles and where we assume a 'standard' ensemble of particles initially distributed over one wavelength of the flow. It is straighforward to prove that this gives the same result as using the index $i(t)$ in the limit as $t \to \infty$. First note that since there is no net flux along the layer, $\langle x(t)-x(0)\rangle = 0$ and can be ignored in (3.17). Next, note that we may write $x(t) = \frac{1}{2}Xi(t) + \xi(t)$, where $\xi(t)$ is bounded by the size of the cell. Then

$$2t\gamma d_{\mathrm{num}}(t) = \tfrac{1}{4}X^2\langle (i(t)-i(0))^2\rangle + X\langle (i(t)-i(0))(\xi(t)-\xi(0))\rangle + \langle (\xi(t)-\xi(0))^2\rangle. \tag{3.18}$$

The second, correlation term decays to zero for large t, whilst the third term is small and bounded for all t: neither contributes to (3.17) as the limit of infinite time is approached. Thus the limiting behaviour obtained by using the true particle

coordinates will give the same result as that obtained by using only the cell index of each particle. This is confirmed by numerical calculations. However, it is clear that the value $\gamma d_{\text{num}}(T)$ after one period, T, of the flow is altered by the presence of the two extra terms; it is important to recognize that when $\gamma d_{\text{num}}(T)$ is used to estimate $\gamma D'_{\text{M}}$, then the cell index of particles, rather than their absolute coordinate, must be used. Numerical computations confirm that $\langle (x(T)-x(0))^2 \rangle > \frac{1}{4}X^2 \langle (i(T)-i(0))^2 \rangle$ for all parameter values investigated.

We summarize the results of this section as follows. In numerical calculations based on an ensemble of particles initially distributed evenly throughout one wavelength of the flow, the true diffusion coefficient D satisfies

$$\gamma D = \gamma D_{\text{num}} = \lim_{t \to \infty} \gamma d_{\text{num}}(t); \tag{3.19}$$

our estimate of the diffusion coefficient from (3.12) satisfies

$$\begin{aligned} \gamma D_{\text{M}} &= \frac{2\lambda}{1+\lambda^2} \gamma d_{\text{num}}(T) \\ &= \gamma d_{\text{num}}(T) \quad \text{when} \quad \lambda = 1, \end{aligned} \tag{3.20}$$

provided $\gamma d_{\text{num}}(t)$ is calculated using the cell index of particles, and not their absolute x-coordinate.

4. More complicated configurations

The calculations described in §3 estimate the longitudinal diffusion coefficient for two-dimensional flows subject to a time-periodic perturbation. In practice, however, the geometry of the flow is likely to be more complicated than this idealized description. For example, the instability of the basic flow might take the form of a perturbation which is periodic in the third spatial coordinate (e.g. wavy instability of convection rolls) or the basic flow itself might be three-dimensional (e.g. Taylor vortices). These more complicated situations can be studied by applying the general principles of the method described in §3.

When the basic flow is three-dimensional, the stagnation points are replaced by one-dimensional curves. The manifolds of these curves, and likewise the boundaries between adjacent cells, are two-dimensional surfaces. Then the probability of changing cells is governed by the volume contained between intersections of these manifolds in the three-dimensional Poincaré map, and the volume of the mixing region of the cells, just as the equivalent areas governed the diffusion in the two-dimensional case. In a rectangular geometry these volumes are infinite, although their ratio is finite: we should more rigorously refer to the mean of the corresponding areas on cross-sections cutting through the cells. When the velocity is independent of the coordinate along the rolls, all such cross-sections are identical, and the problem reduces to the two-dimensional case. Note, however, that flows in cylindrical geometries, such as the Taylor-vortex flow, should not be reduced to two dimensions in this way since the curvature of the problem destroys the area-preservation of the 'reduced' two-dimensional flow. This is illustrated in the discussion of numerical results in §5.

When the perturbation is periodic in the coordinate along the roll, z say, time can be eliminated to give a system of two coupled equations. Thus given

$$\dot{x} = u(x, y, z), \quad \dot{y} = v(x, y, z), \quad \dot{z} = w(x, y, z),$$

we write
$$\frac{\mathrm{d}x}{\mathrm{d}x} = \frac{u}{w}, \quad \frac{\mathrm{d}y}{\mathrm{d}z} = \frac{v}{w},$$

provided $w \neq 0$. Note that although the original three-dimensional flow preserves volume, this reduced two-dimensional flow does not, in general, preserve area. A Melnikov function can be calculated as in §3: however, the integral (2.4) must be modified to allow for changes in areas, as described by Holmes (1980). This Melnikov function describes the separation of the two-dimensional manifolds in the full, three-dimensional, space of the flow. From this, the volume of fluid changing cell whilst travelling downstream a distance equal to one period of the perturbation can be found. In this case, the coefficient describes the rate of diffusion with distance along the roll rather than with time. This may be of use in particular applications. However, when the rate of diffusion with time is of more direct interest, this might be estimated by renormalizing by the average speed along the rolls.

5. Comparison with numerical results

As an example, we consider the model of cylinder waves in Taylor-vortex flow introduced by Broomhead & Ryrie (1988). We evaluate the expression for our approximation to the diffusion coefficient, and compare this with numerical results.

The velocity field of the flow is

$$\left.\begin{aligned} \dot{r} &= \frac{\pi(r+\frac{1}{2})(r-\frac{1}{2})}{R+r}\cos(\pi z), \\ \dot{\theta} &= A + \frac{B}{(R+r)^2}, \\ \dot{z} &= -\frac{2r}{R+r}\sin(\pi z) - \epsilon\sin(\omega t) \end{aligned}\right\} \tag{5.1}$$

in cylindrical polar coordinates, where $r \in [-\frac{1}{2}, \frac{1}{2}], \theta \in [0, 2\pi)$, $z \in (-\infty, +\infty)$. The parameter R is the mean radius of the cylinders, which have true radii $(R-\frac{1}{2})$ and $(R+\frac{1}{2})$. In the unperturbed flow, $\epsilon = 0$, particles are confined to surfaces of constant $\psi(r,z) = (r+\frac{1}{2})(r-\frac{1}{2})\sin(\pi z)$. Curves of constant $\psi(r,z)$ are shown in figure 5. The vortex boundaries lie at $z = n$ (integer n), and the Melnikov function at the boundary is, following Broomhead & Ryrie (1988),

$$M_n(r_0, t_0) = \frac{(-1)^n}{(R+r_0)}|I_n|\sin(\omega t_0 + \phi + \eta(r_0)), \tag{5.2}$$

where
$$I_n = 2R\Gamma(1+\alpha)\Gamma(1+\beta)/\Gamma(3+\alpha+\beta),$$

and
$$\phi = \arg(I_n), \quad \alpha = \frac{(-1)^{n+1}\mathrm{i}\omega(R-\frac{1}{2})}{\pi}, \quad \beta = \frac{(-1)^n\mathrm{i}\omega(R+\frac{1}{2})}{\pi},$$

$$\eta(r_0) = (-1)^n\frac{\omega}{\pi}[(R-\tfrac{1}{2})\ln(\tfrac{1}{2}+r_0) - (R+\tfrac{1}{2})\ln(\tfrac{1}{2}-r_0)].$$

In fact
$$|I_n|^2 = \frac{4\pi^4R^2}{(4\pi^2+\omega^2)(\pi^2+\omega^2)}\frac{\omega(R-\frac{1}{2})}{\sinh[\omega(R-\frac{1}{2})]}\frac{\omega(R+\frac{1}{2})}{\sinh[\omega(R+\frac{1}{2})]}\frac{\sinh(\omega)}{\omega}, \tag{5.3}$$

independent of n: the Melnikov function is the same at all boundaries, apart from a change of sign. This is a direct consequence of the invariance of (5.1) under

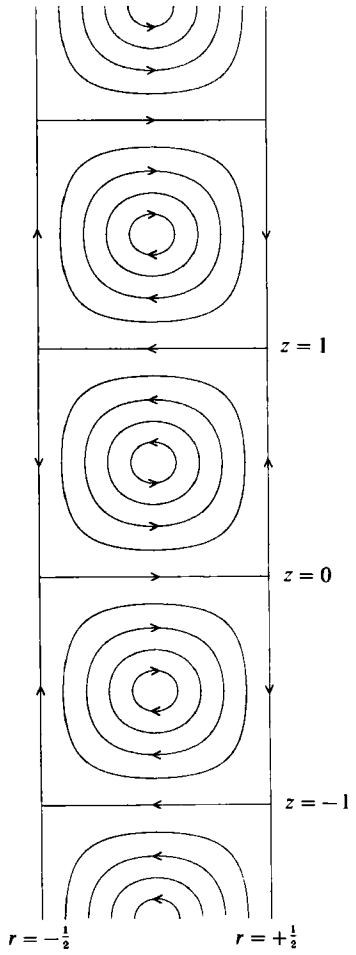

FIGURE 5. Curves of constant $\psi(r, z) = (r+\frac{1}{2})(r-\frac{1}{2})\sin(\pi z)$, i.e. intersections with θ = constant of invariant surfaces for the model Taylor-vortex flow with $\epsilon = 0$.

the transformation $(r, \theta, z, t) \to (r, -\theta, z+\pi, -t)$. Note that this invariance implies that both cells have identical structures, so that the Markov model predicts $\gamma D_{\mathrm{M}} = \gamma d_{\mathrm{num}}(T)$ as discussed in §3.

The volume of fluid crossing the cell boundary near $z = n$ during one period of the flow is then

$$V_n = \left| \int_{\Gamma_{01}}^{\Gamma_{02}} 2\pi (R + r_0) \frac{\epsilon M_n(r_0, t_0)}{|\dot{r}(r_0, n)|} \mathrm{d}r_0 \right| + O(\epsilon^2),$$

where r_{01} and r_{02} are succcssive zeros in r_0 of $M_n(r_0, t_0)$. Thus

$$\begin{aligned} V_n &= \epsilon\, 2\pi |I_n| \left| \int_{r_{01}}^{r_{02}} \sin(\omega t_0 + \phi + \psi(r_0)) \frac{\mathrm{d}t_0}{\mathrm{d}r_0} \mathrm{d}r_0 \right| + O(\epsilon^2) \\ &= \epsilon\, 2\pi |I_n| \left| \int_{t_{01}}^{t_{01}+\pi/\omega} \sin(\omega t_0 + \phi + \psi(r_0))\, \mathrm{d}t_0 \right| + O(\epsilon^2) \\ &= \epsilon \frac{4\pi}{\omega} |I_n| + O(\epsilon^2) \quad \text{as} \quad \epsilon \to 0, \end{aligned} \tag{5.4}$$

where t_{01} and $t_{01}+\pi/\omega$ are successive zeros in t_0 of $M_n(r_0, t_0)$. It follows from (3.12) that our estimate of the diffusion coefficient for this flow is

$$D_{\mathrm{M}} = 2^2 \frac{\omega}{2\pi} \frac{V_n V_{n+1}}{V_n + V_{n+1}} \frac{1}{V_{\mathrm{mix}}} \tag{5.5}$$

where V_{mix} is the volume of cells n and $(n+1)$ in which the flow is chaotic. Writing $V_{\mathrm{mix}} = \gamma 4\pi R$, where γ is the proportion of the flow which is chaotic, we have

$$D_{\mathrm{M}} = \frac{1}{\gamma} \frac{\epsilon |I_n|}{\pi R} + O(\epsilon^2) \quad \text{as} \quad \epsilon \to 0. \tag{5.6}$$

For the parameter values $\omega = \frac{1}{4}$, $R = 5$ we find $|I_n| = 3.9$ and predict $\gamma D_{\mathrm{M}} = 0.25\epsilon + O(\epsilon^2)$. Broomhead & Ryrie (1988) found γD numerically for these parameter values by computing $\gamma d_{\mathrm{num}}(t) = \langle (z(t)-z(0))^2 \rangle / 2t$ for an ensemble of particles initially distributed evenly in the plane $\theta = 0$, with $r \in [-\frac{1}{2}, \frac{1}{2}]$, $z \in [-1, 1]$. Thus they essentially treated the problem of diffusion in the (r, z)-plane. However, the flow in this decoupled system is not area-preserving, as discussed in §4: a more appropriate ensemble for our purposes would be one comprising particles evenly distributed throughout the entire volume of fluid, or, equivalently, distributed in (r, z)-space with density $\rho(r) \propto (R+r)$. We might expect the effects of this discrepancy to be small, particularly for large R, and continue with the comparison.

Broomhead & Ryrie identified three distinct regions in the graph of $\gamma d_{\mathrm{num}}(t)$.

(i) $0 < t < t_0$: $\gamma d_{\mathrm{num}}(t) \propto t$. This is the deterministic regime in which particles retain memory of their past history. Typically they found $t_0 \approx \frac{1}{2}T$.

(ii) $t_0 < t < t_1$: $\gamma d_{\mathrm{num}}(t)$ falls rapidly to a minimum of $\bar{D}$, then may oscillate close to this value. The value of t_1 varied considerably with the parameters of the flow, and in particular with ϵ, so that no consistent trend was apparent. However, the minimum, $\bar{D}$, was normally achieved at a time $t \approx T$, so that it is consistent with their results to interpret $\bar{D}$ as $\gamma d_{\mathrm{num}}(T)$. We choose to do this henceforth since the significance of this quantity is then more apparent. Note, however, that their computations used the z-coordinate rather than cell index of each particle, so we expect $\gamma d_{\mathrm{num}}(T)$ to be consistently larger than γD_{M} as discussed in §3.

(iii) $t > t_1$: $\gamma d_{\mathrm{num}}(t)$ may increase or decrease to a limiting value γD_{num} (which may be equal to $\gamma d_{\mathrm{num}}(T)$), or may increase without limit. This latter behaviour is likely to be due to the presence of 'accelerator modes' such as those found in the standard map (cf. Lichtenberg & Lieberman 1983).

Figure 6 shows our theoretical result for γD_{M} (equation (5.6)) superposed on the graph of $\gamma d_{\mathrm{num}}(T)$ *and* γD_{num} versus ϵ, reproduced from figure 15 of Broomhead & Ryrie (1988). New results of $\gamma d_{\mathrm{num}}(T)$ based on the correct initial distribution of 10000 particles, and using the cell index are also shown. The behaviour of γD_{num} is complicated and does not agree well with the theory over most of the range $0 \leqslant \epsilon \leqslant 0.1$. However, for $\epsilon \leqslant 0.01$, $\gamma D_{\mathrm{num}} \equiv \gamma d_{\mathrm{num}}(T)$, and the agreement is good. In addition, the agreement between $\gamma d_{\mathrm{num}}(T)$ and the theory is reasonable over the entire range, as we would expect from the discussion at the end of §3.

The computations were repeated for parameter values $\omega = \frac{1}{4}, R = 2$, and with the correct distribution of particles in the (r, z)-plane: 5120 particles were used for long-timescale computations of γ and D_{num}, whilst 10240 were used for the short-time computations of $\gamma d_{\mathrm{num}}(T)$. For these parameter values we predict $\gamma D_{\mathrm{M}} = 0.32\epsilon + O(\epsilon^2)$ as $\epsilon \to 0$. This time the function $\gamma d_{\mathrm{num}}(t) = X^2 \langle (i(t)-i(0))^2 \rangle / 8t$, where i denotes the cell occupied by the particle, was computed. In some cases we

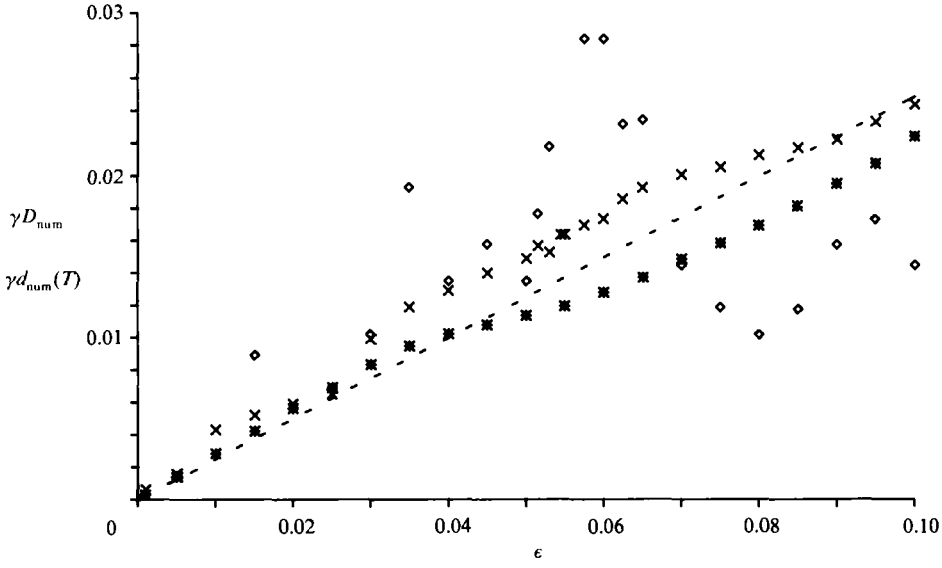

FIGURE 6. Numerical results for $\gamma d_{\rm num}(T)$ ($\times$) and $\gamma D_{\rm num} = \lim_{t\to\infty} \gamma d_{\rm num}(t)$ ($\diamond$) versus ϵ, reproduced from figure 15 of Broomhead & Ryrie (1988), for the model Taylor-vortex flow with $\omega = \frac{1}{4}$, $R = 5$. Also shown is $\gamma d_{\rm num}(T)$ ($*$) computed using the cell index of particles, and for the correct initial distribution of 10240 particles. The dashed line shows the value $\gamma \bar{D} = 0.25\epsilon$ predicted by our analytical model.

found that $d_{\rm num}(t)$ remained close to $d_{\rm num}(T)$ for a short time ($\lesssim 6T$), whilst in others it immediately increased. The results are shown in figure 7(*a*), where $\gamma \bar{D}_{\rm M} = 0.32\epsilon$, $\gamma d_{\rm num}(T)$ and $\gamma D_{\rm num}$ are plotted against ϵ. For $\epsilon < 0.015$, $\gamma d_{\rm num}(T)$ is close to 0.32ϵ as expected; however, for $\epsilon > 0.015$, $d_{\rm num}(T)$ diverges from this linear approximation, indicating that the Melnikov function does not accurately measure the distance between the perturbed manifolds there. The behaviour of $\gamma D_{\rm num}$ is again complicated, though the underlying trend is oscillatory; for values of ϵ close to multiples of 0.007, $\gamma D_{\rm num}$ was not always defined, owing to the presence of accelerator modes. For small ϵ, $\gamma D_{\rm num}$ is consistently larger than $\gamma d_{\rm num}(T)$: however, for $\epsilon > 0.07$, $\gamma d_{\rm num}(T)$ and $\gamma D_{\rm num}$ agree quite closely, indicating that the Markov formulation is a good approximation there. It is interesting to note that at these larger values of ϵ no accelerator modes were observed. This behaviour is similar to that observed in the standard map (cf. Lichtenberg & Lieberman 1983), where the oscillations in the diffusion coefficient decay as the parameter K is increased, tending to the quasi-linear result as $K \to \infty$.

The proportion of the flow which is chaotic, γ, is shown in figure 7(*b*). For $\epsilon < 0.065$, $\gamma \propto \epsilon^p$ where $p \approx 0.65$: if we limit ϵ to $\epsilon < 0.030$ a rather better fit gives $p \approx 0.67$. At $\epsilon \approx 0.065$ there is a sudden increase in the slope of the graph of γ versus ϵ. This corresponds to the graph of $\gamma D_{\rm num}$ saturating to an approximately constant value. The net effect is that the diffusion coefficient, $D_{\rm num}$, increases, initially as $\epsilon^{0.33}$ and then more slowly, to a maximum at $\epsilon \approx 0.065$, and thereafter decreases.

The accuracy of our numerical results was checked by computing $\gamma d_{\rm num}(t)$ for ten different (randomly selected) sets of 1023 particles, with $\epsilon = 0.1$ and 0.05. From these results the function $\gamma d_{\rm num}(t)$ for any set of $n \times 1023$ ($n = 1, 2, \ldots, 10$) particles could be reconstructed, thus allowing the effects of altering the total number of particles, and the initial positions for a given number of particles, to be tested. We found that the estimates of $\gamma D_{\rm num}$ for the ten sets of 1023 particles had a standard

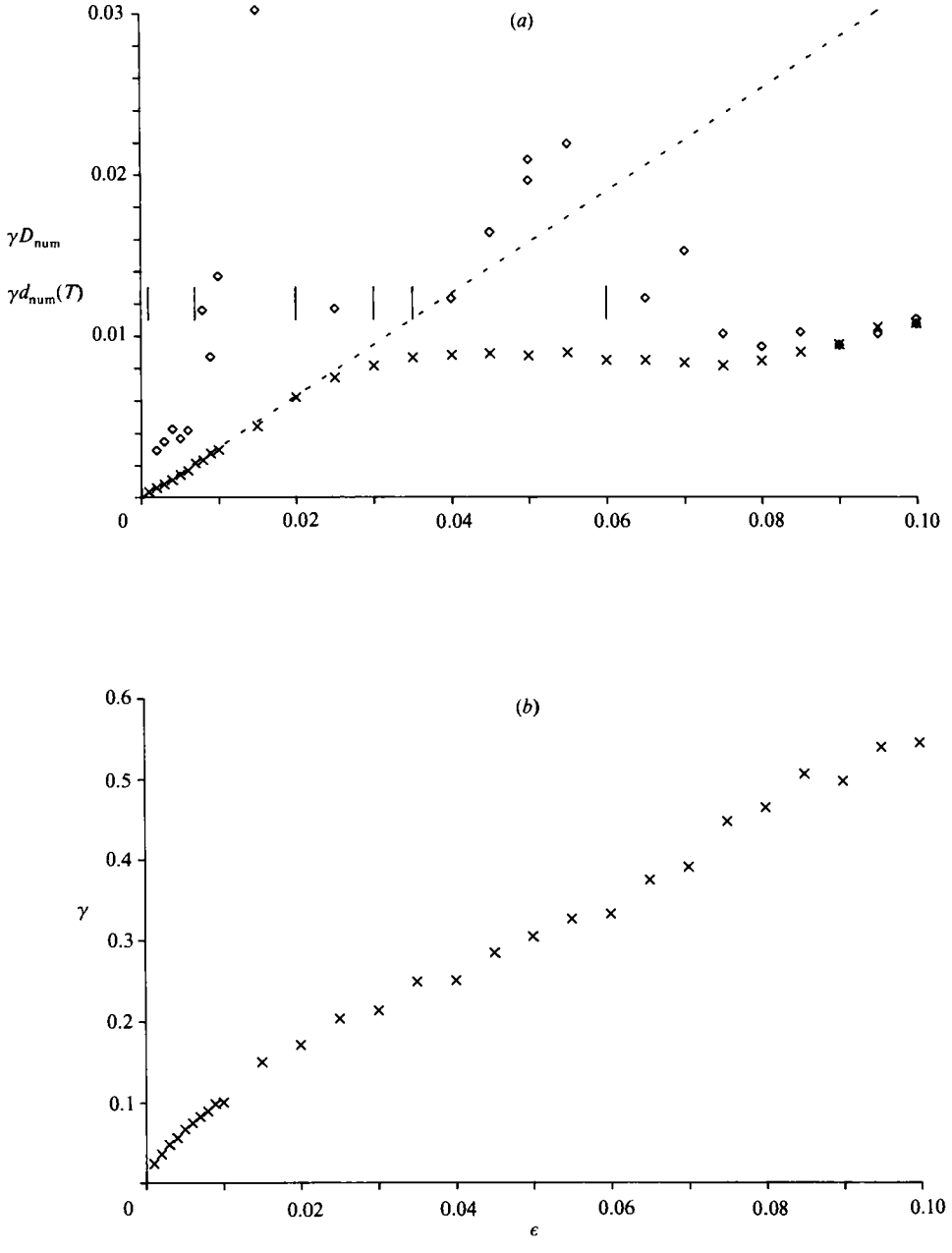

FIGURE 7. (*a*) Numerical results for $\gamma d_{\text{num}}(T)$ ($\times$, 10240 particles) and $\gamma D_{\text{num}} = \lim_{t\to\infty} \gamma d_{\text{num}}(T)$ ($\diamond$, 5120 particles) versus ϵ for the model Taylor-vortex flow with $\omega = \frac{1}{4}$, $R = 2$. Vertical bars denote the presence of accelerator modes. The dashed line shows the value $\gamma \bar{D}_{\text{M}} = 0.32\epsilon$ predicted by the analytical model together with the Melnikov estimate of the $a_{i,j}$. At $\epsilon = 0.05$ and $\epsilon = 0.10$, two values of γD_{num}, computed using different sets of initial conditions, are shown to indicate the expected size of numerical errors. (*b*) Proportion of the flow, γ, which is chaotic (calculated using 5120 particles) versus ϵ. Note the sudden change in slope near $\epsilon = 0.065$.

deviation of 7% of their mean at $\epsilon = 0.1$ and 9% at $\epsilon = 0.05$; the estimates for different sets of 2046 particles had a standard deviation of 5% of their mean value at $\epsilon = 0.1$ and 7% at $\epsilon = 0.05$. The estimates of γ had lower standard deviations of around 5% for 1023 particles and 3% for 2046 particles, for both values of ϵ. In both cases the results appeared to have converged for $n = 6$, i.e. for sets of 6138 particles. Thus we may be reasonably confident of the accuracy of the results shown in figure 7(*a*), computed using 5120 particles: some indication of the size of the errors there is given by plotting γD_{num} and γ for two different sets of initial conditions at $\epsilon = 0.05$ and 0.10.

6. Flows with non-zero net flux

The Markov model described in §3 can be generalized to situations in which there is a net flux of fluid along the layer. Thus following (3.9) we may define the probability of a particle migrating from cell i to cell j in one 'step' as

$$P_{i,j} = \begin{cases} (1-a-b)\,\delta_{j,i} + a\delta_{j,i+1} + b\delta_{j,i-1}, & i \text{ even} \\ (1-c-d)\,\delta_{j,i} + c\delta_{j,i+1} + d\delta_{j,j-1}, & i \text{ odd} \end{cases} \tag{6.1}$$

for some $a, b, c, d, \in [0, 1]$ such that $(a+b) \in [0, 1]$ and $(c+d) \in [0, 1]$. The model of §3 can be regained by setting $a = \rho$, $b = \lambda\rho$, $c = \mu\lambda\rho$ and $d = \mu\rho$. In order to satisfy the condition of incompressibility of the fluid we require

$$\mu(a+b) = (c+d), \tag{6.2}$$

where $\mu = A_{2r}/A_{2r+1}$ as in §3: the net flux of fluid along the layer is

$$\phi \propto \mu a - d = c - \mu b. \tag{6.3}$$

The averages $\langle i \rangle_n$, $\langle i\, i_0 \rangle_n$ and $\langle i^2 \rangle_n$ are most easily calculated by using a matrix notation to calculate

$$\boldsymbol{I}_n^k \overset{\text{def}}{=} \begin{pmatrix} \sum_r (2r)^k p_{2r}^n \\ \\ \sum_r (2r+1)^k p_{2r+1}^n \end{pmatrix}, \tag{6.4}$$

where p_i^n is the probability of a particle being in state i after n steps of the Markov process (cf. Appendix). Then we find

$$\begin{aligned} \boldsymbol{I}_{n+1}^0 &= \boldsymbol{A}\boldsymbol{I}_n^0, \\ \boldsymbol{I}_{n+1}^1 &= \boldsymbol{A}\boldsymbol{I}_n^1 + \boldsymbol{B}\boldsymbol{I}_n^0, \\ \boldsymbol{I}_{n+1}^2 &= \boldsymbol{A}\boldsymbol{I}_n^2 + 2\boldsymbol{B}\boldsymbol{I}_n^1 + \boldsymbol{C}\boldsymbol{I}_n^0, \end{aligned} \tag{6.5}$$

where

$$\boldsymbol{A} = \begin{pmatrix} 1-a-b & c+d \\ a+b & 1-c-d \end{pmatrix}, \quad \boldsymbol{B} = \begin{pmatrix} 0 & c-d \\ a-b & 0 \end{pmatrix}, \quad \boldsymbol{C} = \begin{pmatrix} 0 & c+d \\ a+b & 0 \end{pmatrix};$$

the averages are given by

$$\langle i \rangle_n = (1 \quad 1)\boldsymbol{I}_n^1, \quad \langle i^2 \rangle_n = (1 \quad 1)\boldsymbol{I}_n^2. \tag{6.6}$$

Solution of (6.5) and (6.6) yields expressions of the form

$$\langle (i-i_0)^2 \rangle_n = \left[\frac{2(ac-bd)}{a+b+c+d}\right]^2 n^2 + \alpha(a, b, c, d, \xi^n)\, n + \beta(a, b, c, d)\,(1-\xi^n), \tag{6.7}$$

and
$$\langle i-i_0\rangle_n = \frac{2(ac-bd)}{a+b+c+d}n+\gamma(a,b,c,d)\,(1-\xi^n), \tag{6.8}$$

for some complicated expressions α, β and γ, and where $\xi = 1-(a+b+c+d)\in[-1, 1]$. Therefore, ignoring the trivial case $\xi = 1$ ($a = b = c = d = 0$) and the special case $\xi = -1$, we find

$$\langle(i-i_0)^2\rangle_n-\langle i-i_0\rangle_n^2 \sim \left[\alpha(a,b,c,d,0)-\frac{2(ac-bd)}{a+b+c+d}\gamma(a,b,c,d)\right]n \quad \text{as} \quad n\to\infty. \tag{6.9}$$

Equation (6.9) is also valid when $\xi = -1$, since then $a+b = c+d = 1$, $\mu = 1$ and $a-b = c-d$; moreover, for a, b, c, d satisfying these constraints $\alpha(a, b, c, d, \xi^n)$ is independent of ξ^n.

Equation (6.9) predicts diffusive-like transport, but no anomalous diffusion. The effect of including a net flux of particles in the Markov model is merely to sweep the spreading cloud downstream at a constant rate; the nature of the dispersion of the cloud is unaffected. Therefore the Markov model alone is unable to explain the anomalous diffusion observed by Weiss & Knobloch (1989) and Cox *et al.* (1990). However, the flows studied by Weiss & Knobloch and Cox *et al.* have an important property which is absent from the Markov model. This is the presence of shear in the main stream: indeed it is difficult to conceive of any flow of interest which does not exhibit shear in the main stream. By contrast the Markov model represents a flow in which the net flux is due to a uniform stream. This suggests that it is the shear in the flow, rather than the net flux itself, which is responsible for the anomalous diffusion. This association of cause and effect was suggested in the work of both Weiss & Knobloch and Cox *et al.*: the results from the generalized Markov model further support this hypothesis.

It is interesting to consider in this context, also, the effect caused by the presence of accelerator modes in flows with zero net flux. As discussed previously, it is likely that the singularities observed in numerical calculations of the diffusion coefficient are due to presence of these modes causing streaming, rather than diffusing, of some particles (cf. Lichtenberg & Lieberman 1983; Broomhead & Ryrie 1988; Weiss & Knobloch 1989). A particle caught in an accelerator mode moves continuously along the layer at a constant rate. Thus a single accelerator mode, or a number of accelerator modes with the same velocity, is equivalent to the presence of a uniform net flow; as such it is unable to produce anomalous diffusion, and hence singularities in the graph of the diffusion coefficient. To further understand this property, consider a transformation which brings to rest those particles moving in the accelerator mode(s). Since the position of these particles does not change they are unable to contribute of a diffusion coefficient. The remaining cloud of particles is swept along at a constant rate in this new frame of reference; the transformation does not affect the dispersion properties of the cloud, or any diffusion coefficient. However, the presence of a number of accelerator modes of different speeds is equivalent to the presence of a net flux with shear in the mean flow. In this case it is not possible to define a transformation which brings to rest all particles trapped in the accelerator modes. The net effect is that the diffusion coefficient receives a contribution from the dispersing cloud, which will tend to a constant at large times, and a contribution from the streaming particles which increases without limit. Thus we observe anomalous diffusion, and singularities in a graph of the diffusion coefficient. It is

unlikely that accelerator modes will occur individually, so that in practice their presence will always lead to anomalous diffusion. This is certainly the case in the standard map, where accelerator modes with all integer multiples of the basic velocity are possible (cf. Lichtenberg & Lieberman 1983, p. 221); and in fluid flows at least two accelerator modes acting in opposite directions are necessary to preserve a condition of no net flux.

7. Conclusions

We have investigated transport by chaotic advection in a general class of spatially periodic flows. Under the approximation that particles in the chaotic region are uncorrelated with their past history, we have shown that the density of test particles obeys a discrete advection–diffusion equation. In addition, by modelling the transport process by a Markov chain we have been able to derive an analytic approximation for the diffusion coefficient. The mechanism for diffusion is the interchange of fluid between vortices through the turnstiles in the cell boundaries. The expression derived for the diffusion coefficient depends upon the area (or volume) of the 'lobes' enclosed by the turnstiles, and the proportion of the domain of the flow which is chaotic.

The numerical results discussed in §5 give some indication of the validity of the approximations used in our model. When the size, ϵ, of the perturbation from the basic integrable flow is small, accelerator modes may be present so that correlation effects are important. Then a graph of the true value of the diffusion coefficient versus ϵ may show large-scale oscillations about our approximate analytic result. In this region our simple model can at best be expected to give only an order of magnitude estimate of the diffusion coefficient. An exception appears to occur at particularly small values of ϵ, before the first accelerator modes occur; then our predicted linear variation, with ϵ, of the spatially averaged diffusion coefficient agrees well with numerical and experimental observations.

For larger values of ϵ, there is some evidence that correlation effects become less important; it is in this region that the Markov model is most accurate. This is demonstrated by the agreement between $\gamma D_{\mathrm{M}} = \gamma d_{\mathrm{num}}(T)$ and γD_{num} when $\epsilon > 0.07$ in figure 7(*a*). Similar behaviour is observed in the standard map, where measured values of the diffusion coefficient approach the quasi-linear result as the parameter K (equivalent to our parameter ϵ) increases towards infinity. Moreover, similar behaviour is indicated in flow around an oscillating vortex pair (Rom-Kedar 1989); numerical results suggest that the probability of escape from the vortex becomes constant with time when the amplitude of the unsteady component of the flow is increased (indirectly through the period of the flow) beyond a critical value.

We expect, then, that the Markov model is most accurate when the flow is not close to integrable. Further investigation is needed to clarify whether this is indeed so, and the reasons for it. It would be interesting in this context to compute autocorrelation functions $\overline{x(t)x(t+\tau)}$ (where the bar denotes an average over time, t) for particle paths, and to test whether the rate of decay of these functions, in comparison with the temporal period of the flow, is indeed important in governing the accuracy of the model, as suggested in §1. It would also be interesting to compute such quantities as Lyapunov exponents (cf. Lichtenberg & Lieberman 1983, p. 262). These govern the rate of divergence of nearby particle paths, and as such could be expected to be related to diffusion coefficients, though probably not in a simple manner. Note that a relationship between Lyapunov exponents and the rate of decay of autocorrelation

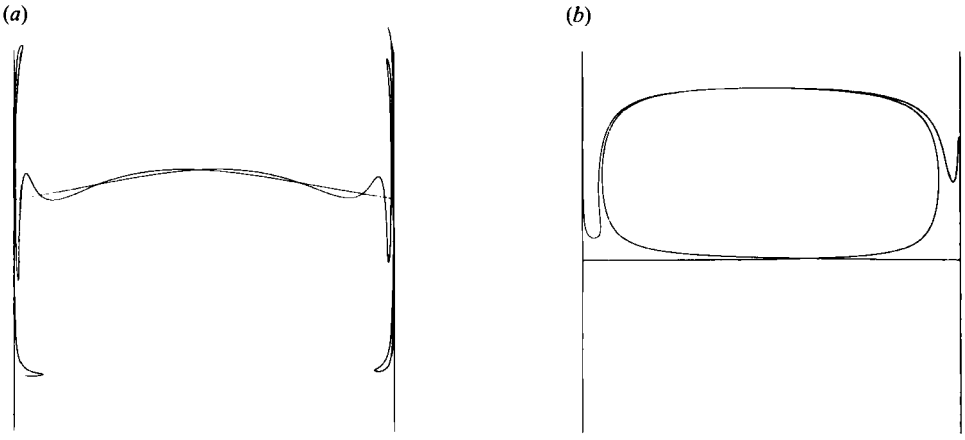

FIGURE 8. Part of the perturbed manifolds near $z = 0$ for the model Taylor-vortex flow. (*a*) $\omega = \frac{1}{4}$, $R = 20$, $\epsilon = 0.1$; the vortex spins slowly, and the lobes have a simple shape. (*b*) $\omega = \frac{1}{4}$, $R = 2$, $\epsilon = 0.05$; the vortex spins rapidly, since R is small and hence $|\dot{r}|$ and $|\dot{z}|$ large. The manifolds are swept around the vortex before intersecting a second time. Hence the lobes have a complicated shape, and their area cannot easily be computed.

functions has already been demonstrated for one- and two-dimensional maps (Badii *et al.* 1988).

The Markov model has enabled us to demonstrate how diffusion-like transport can arise in chaotically advecting flows. It has also shown, along with the work of Rom-Kedar (1989) and Rom-Kedar *et al.* (1990), that the areas of the turnstiles in the cell boundaries are important in determining the rate of mixing in the fluid; moreover it has provided a simple approximation for the diffusion coefficient which explains some features of numerical and experimental observations. However, its usefulness in predicting the diffusion coefficient in practical situations is limited by the difficulties of calculating the areas $a_{i,j}$ of the turnstiles, and the proportion γ of the flow which is mixing. These difficulties are not a particular feature of our model, but are likely to occur in any theory of diffusion in these flows. We consider separately the different quantities.

The calculation of the $a_{i,j}$ was discussed briefly in §3. For a known flow, and for ϵ sufficiently small, the $a_{i,j}$ can be calculated in terms of the Melnikov function at the appropriate cell boundary. However, for larger ϵ the Melnikov function no longer provides an accurate approximation of the distance between the perturbed manifolds, and higher-order terms must be included in the series expansion. In general it is a non-trivial problem to carry out this extension analytically, and numerical methods of calculating the areas might be preferred. It is straightforward to compute the positions of the perturbed manifolds, and hence the areas $a_{i,j}$, in cases where the shape of the lobes $I_{i,j}$ is simple (e.g. for the model of Taylor-vortex flow with parameters $\omega = \frac{1}{4}$, $R = 20$ and $\epsilon = 0.1$ as shown in figure 8*a*). However, in other cases the shape of the lobes may be quite complicated; figure 8(*b*) shows an example where the lobe is wound round the rapidly spinning vortex, making any numerical calculation of its area quite difficult.

When numerical methods must be used it is often easier to calculate the quantity $\gamma d_{\mathrm{num}}(T)$ rather than the a_{ij}, as discussed in §3. Then for flow with special symmetries such that $\lambda = 1$, $\gamma d_{\mathrm{num}}(T) \equiv \gamma D_{\mathrm{M}}$. Of course care must be taken to ensure that the ensemble used is sufficiently large to give an accurate result.

The calculation of γ is even more problematical. In general there is no analytic method of calculating this quantity. Moreover, numerical calculations require that the paths of large numbers of particles be computed for large times, in order to distinguish between particles that are free to move along the layer and those that remain trapped indefinitely in the cores of the cells; this is computationally expensive! The exception in which this problem does not arise is when ϵ is sufficiently large that the entire flow is mixing, and $\gamma \equiv 1$. Of course, as we discussed in §3, it is sometimes more appropriate to consider the spatial average, over the entire flow, of the diffusion coefficient, i.e. the quantity γD rather than D. However, this does not avoid the need to calculate γ, since a knowledge of D or γD alone is not sufficient to completely characterize the mixing of the flow. In order to do this it is necessary to know both the proportion of the flow that is mixing, and the rate at which this mixing occurs. Thus γ and D must both be provided by any complete theory of mixing, since they separately provide important, and distinct measures of the mixing.

At present, an improvement of our theory by obtaining expressions for the $a_{i,j}$ and for γ does not appear to be feasible. A more tractable problem might be to include correlation effects, which are the main source of inaccuracy of the Markov model. The transport of the particles depends not only on the areas of individual lobes, but upon the 'tangible dynamics' of lobes, that is, upon the way lobes intersect one another (Rom-Kedar 1989 and Rom-Kedar *et al.* 1990). To include these effects in calculations of diffusion coefficients is also a non-trivial extension of the work reported here, and would greatly increase the complexity of the problem.

Throughout this study we have been concerned with the motion of ideal fluid particles, and hence the mixing within a homogeneous fluid. It is important to realize that in some situations additional effects should be taken into consideration. For example, when the particles have a finite size, such as in the transport of sediments and some pollutants, they move relative to the fluid; or molecular diffusion might be present, such as in the dispersion of a solute or the mixing of two fluids. The different velocity experienced by particles of a finite size might cause them to follow paths quite different from those of the fluid particles, and dissipation effects are likely to lead to the presence of attracting solutions in the phase space. The effects of molecular diffusion are likely to be less dramatic, however, since in most cases the mixing by chaotic advection is expected to occur on a much faster timescale (Cox *et al.* 1990).

I am grateful to Dr D. S. Broomhead for interesting discussions regarding diffusion in the Taylor-vortex flow: they provided the basis from which this work has evolved. Also, I would like to thank Professor P. G. Drazin for much advice and encouragement and Dr E. J. Collins for useful discussions. This work was supported financially by SERC.

Appendix. Calculation of moments in the Markov model

The longitudinal transport of particles was modelled by a Markov process, in which the probability of changing from state i to state j, $P_{i,j}$, is

$$P_{i,j} = \begin{cases} \lambda\rho\delta_{j,i-1} + (1-\rho-\lambda\rho)\,\delta_{j,i} + \rho\delta_{j,i+1}, & i \text{ even} \\ \mu\rho\delta_{j,i-1} + (1-\mu\rho-\mu\lambda\rho)\,\delta_{j,i} + \mu\lambda\rho\delta_{j,i+1}, & i \text{ odd.} \end{cases} \tag{A 1}$$

(An introduction to Markov processes, and their relationship to diffusion processes

can be found in, for example, Cox & Miller 1965.) Consider a single particle, and denote the probability of it being in state i after n steps by p_i^n. Then after $n+1$ steps,

$$\left.\begin{aligned} p_{2r}^{n+1} &= (1-\rho-\lambda\rho)\,p_{2r}^n+\mu\rho p_{2r+1}^n+\mu\lambda\rho p_{2r-1}^n,\\ p_{2r+1}^{n+1} &= (1-\mu\rho-\mu\lambda\rho)\,p_{2r+1}^n+\lambda\rho p_{2r+2}^n+\rho p_{2r}^n. \end{aligned}\right\} \tag{A 2}$$

Hence the expected value of i^m after n steps is

$$\langle i_m\rangle_n = \sum_i i^m p_i^n, \tag{A 3}$$

and after $n+1$ steps is

$$\begin{aligned} \langle i^m\rangle_{n+1} &= \sum_i i^m p_i^{n+1}\\ &= \langle i^m\rangle_n+\rho\sum_r[\lambda(2r-1)^m+(2r+1)^m-(1+\lambda)(2r)^m]\,p_{2r}^n\\ &\quad+\mu\rho\sum_r[(2r)^m+\lambda(2r+2)^m-(1+\lambda)(2r+1)^m]\,p_{2r+1}^n. \end{aligned} \tag{A 4}$$

The recurrence relations (A 2) and (A 4) can be used to calculate explicit expressions for the expected values, as follows.

(*a*) $m=1$

$$\langle i\rangle_{n+1} = \langle i\rangle_n+\rho(1-\lambda)\sum_r[p_{2r}^n-\mu p_{2r+1}^n]. \tag{A 5}$$

From (A 2),

$$\sum_r[p_{2r}^{n+1}-\mu p_{2r+1}^{n+1}] = [1-\rho(1+\lambda)(1+\mu)]\sum_r[p_{2r}^n-\mu p_{2r}^n], \tag{A 6}$$

whence

$$\sum_r[p_{2r}^n-\mu p_{2r+1}^n] = [1-\rho(1+\lambda)(1+\mu)]^n(\sigma_e^0-\mu\sigma_o^0), \tag{A 7}$$

where

$$\sigma_e^m = \sum_r(2r)^m p_{2r}^0, \quad \sigma_0^m = \sum_r(2r+1)^m p_{2r+1}^0. \tag{A 8}$$

On substituting (A 7) into (A 5) and solving the recurrence relation we find

$$\langle i\rangle_n = \langle i\rangle_0+\rho(1-\lambda)\frac{1-\beta^n}{1-\beta}(\sigma_e^0-\mu\sigma_o^0), \tag{A 9}$$

where

$$\beta = [1-\rho(1+\lambda)(1+\mu)]. \tag{A 10}$$

In the limit as $n\to\infty$, the expected value of i converges to

$$\langle i\rangle_\infty = \langle i\rangle_0+\rho\frac{1-\lambda}{1-\beta}(\sigma_e^0-\mu\sigma_o^0). \tag{A 11}$$

(*b*) $m=2$

$$\langle i^2\rangle_{n+1} = \langle i^2\rangle_n+2\rho(1-\lambda)\sum_r[2rp_{2r}^n-\mu(2r+1)p_{2r+1}^n]+\rho(1+\lambda)\sum_r[p_{2r}^n+\mu p_{2r+1}^n]. \tag{A 12}$$

From (A 2)

$$\sum_r [p_{2r}^{n+1} + \mu p_{2r+1}^{n+1}] = \sum_r [p_{2r}^n + \mu p_{2r+1}^n] - \rho(1+\lambda)(1-\mu)\sum_r [p_{2r}^n - \mu p_{2r+1}^n]. \quad \text{(A 13)}$$

On substituting from (A 7) and solving the recurrence relation we find, on using $\sigma_e^0 + \sigma_o^0 = 1$,

$$\sum_r [p_{2r}^n + \mu p_{2r+1}^n] = \frac{2\mu}{1+\mu} + \frac{1-\mu}{1+\mu}(\sigma_e^0 - \mu\sigma_o^0)\beta^n. \quad \text{(A 14)}$$

Also, $$\sum_r [2r\, p_{2r}^{n+1} - \mu(2r+1)\, p_{2r+1}^{n+1}] = \beta \sum_r [2r\, p_{2r}^n - \mu(2r+1)\, p_{2r+1}^n] - \mu\rho(1-\lambda), \quad \text{(A 15)}$$

whence $$\sum_r [2r\, p_{2r}^n - \mu(2r+1)\, p_{2r+1}^n] = \beta^n(\sigma_e^1 - \mu\sigma_o^1) - \mu\rho(1-\lambda)\frac{1-\beta^n}{1-\beta}. \quad \text{(A 15)}$$

Now substituting (A 14) and (A 16) into (A 12) and solving, we find

$$\langle i^2 \rangle_n = \langle i^2 \rangle_0 + \frac{2\mu}{1+\mu}\frac{4\lambda\rho}{1+\lambda} n + \gamma \frac{1-\beta^n}{1-\beta}, \quad \text{(A 17)}$$

where $$\gamma = \rho(1+\lambda)\frac{1-\mu}{1+\mu}(\sigma_e^0 - \mu\sigma_o^0) + 2\rho(1-\lambda)(\sigma_e^1 - \mu\sigma_o^1) + 2\mu\rho^2\frac{(1-\lambda)^2}{1-\beta}. \quad \text{(A 18)}$$

It is best to eliminate $\langle i^2 \rangle_0$ by calculating $\langle (i-i_0)^2 \rangle$, where i_0 is the initial value of i for a given orbit. Then since

$$\langle i i_0 \rangle_n = \langle i_0^2 \rangle + \rho(1-\lambda)\frac{1-\beta^n}{1-\beta}(\sigma_e^1 - \mu\sigma_o^1), \quad \text{(A 19)}$$

$$\begin{aligned} \langle (i-i_0)^2 \rangle_n &= \langle i^2 \rangle_n - 2\langle i i_0 \rangle_n + \langle i_0^2 \rangle_n \\ &= \frac{2\mu}{1+\mu}\frac{2\lambda}{1+\lambda} 2\rho n + \gamma' \frac{1-\beta^n}{1-\beta}, \end{aligned} \quad \text{(A 20)}$$

where $\gamma' = \gamma - 2\rho(1-\lambda)(\sigma_e^1 - \mu\sigma_o^1)$. Thus $\langle (i-i_0)^2 \rangle_n \sim 2D'n$ as $n \to \infty$: we have a diffusion process with coefficient $D' = \rho 2\mu(1+\mu)^{-1} 2\lambda(1+\lambda)^{-1}$.

REFERENCES

Aref, H. 1984 Stirring by chaotic advection. *J. Fluid Mech.* **143**, 1–22.

Arnol'd, V. I. 1965 Sur la topologie des écoulements stationnaires des fluides parfaits. *C. R. Acad. Sci. Paris* **261**, 17–20.

Badii, R., Heinzelmann, K., Meier, P. F. & Politi, A. 1988 Correlation functions and generalized Lyapunov exponents. *Phys. Rev.* A **37**, 1323–1328.

Broomhead, D. S. & Ryrie, S. C. 1988 Particle paths in wavy vortices. *Nonlinearity* **1**, 409–434.

Chaiken, J., Chevray, R., Tabor, M. & Tan, Q. M. 1986 Experimental study of Lagrangian turbulence in Stokes flow. *Proc. R. Soc. Lond.* A **408**, 165–174.

Clever, R. M. & Busse, F. H. 1974 Transition to time-dependent convection. *J. Fluid Mech.* **65**, 625–645.

Cox, D. R. & Miller, H. D. 1965 *The Theory of Stochastic Processes.* Chapman and Hall.

Cox, S. M., Drazin, P. G., Ryrie, S. C. & Slater, K. 1990 Chaotic advection of irrotational flows and of waves in fluids. *J. Fluid Mech.* **214**, 517–534.

Davey, A., DiPrima, R. C. & Stuart, J. T. 1968 On the instability of Taylor vortices. *J. Fluid Mech.* **31**, 17–52.

DOMBRE, T., FRISCH, U., GREENE, J. M., HÉNON, M., MEHR, A. & SOWARD, A. 1986 Chaotic streamlines in the ABC flows. *J. Fluid Mech.* **167**, 353–392.

GUCKENHEIMER, J. & HOLMES, P. 1983 *Nonlinear Oscillations, Dynamical Systems and Bifurcations of Vector Fields*. Springer.

HÉNON, M. 1966 Sur la topologie des lignes courant dans un cas particulier. *C. R. Acad. Sci. Paris* **262**, 312–314.

HOLMES, P. J. 1980 Averaging and chaotic motions in forced oscillations. *SIAM J. Appl. Maths* **38**, 65–80.

LICHTENBERG, A. J. & LIEBERMAN, M. A. 1983 *Regular and Stochastic Motion*. Springer.

LICHTENBERG, A. J. & LIEBERMAN, M. A. 1988 Diffusion in two-dimensional mappings. *Physica* **33D**, 211–239.

MACKAY, R. S., MEISS, J. D. & PERCIVAL, I. C. 1984 Transport in Hamiltonian systems. *Physica* **13D**, 55–81.

MEISS, J. D. 1986 Transport near the onset of stochasticity. *Particle Accelerators* **19**, 9–24.

MEISS, J. D. & OTT, E. 1986 Markov tree model of transport in area-preserving maps. *Physica* **20D**, 387–402.

OTTINO, J. M. 1989 *The Kinematics of Mixing: Stretching, Chaos and Transport*. Cambridge University Press.

OTTINO, J. M. 1990 Mixing, chaotic advection, and turbulence. *Ann. Rev. Fluid Mech.* **22**, 207–253.

OTTINO, J. M., LEONG, C. W., RISING, H. & SWANSON, P. D. 1988 Morphological structures produced by mixing in chaotic flows. *Nature* **333**, 419–425.

ROM-KEDAR, V. 1989 Transport in two-dimensional maps. PhD. thesis, California Institute of Technology.

ROM-KEDAR, V., LEONARD, A. & WIGGINS, S. 1990 An analytical study of transport, mixing and chaos in an unsteady vortical flow. *J. Fluid Mech.* **214**, 347–394.

SAGUES, F. & HORSTHEMKE, W. 1986 Diffusive transport in spatially periodic hydrodynamic flows. *Phys. Rev.* A **34**, 4136–4143.

SOLOMON, T. H. & GOLLUB, J. P. 1988 Chaotic particle transport in time-dependent Rayleigh–Bénard convection. *Phys. Rev.* A **38**, 6280–6286.

WEISS, J. B. & KNOBLOCH, E. 1989 Mass transport and mixing by modulated travelling waves. *Phys. Rev.* A **40**, 2579–2589.

YOUNG, W., PUMIR, A. & POMEAU, Y. 1989 Anomalous diffusion of tracer in convection rolls. *Phys. Fluids* A **1**, 462–469.